Active Stabilization of Vehicle-Mounted Phased-Array Antennas

Hamidreza Bolandhemmat, Mohammad Fakharzadeh, Pedram Mousavi, *Member, IEEE*, S. Hamidreza Jamali, Gholamreza Z. Rafi, and Safieddin Safavi-Naeini, *Member, IEEE*

***Abstract*—In this paper, a novel hybrid tracking method for mobile active phased-array antenna systems is developed. The proposed technique consists of a mechanical stabilization loop and a direction-of-arrival (DOA) estimation algorithm, which is based on electronic beamforming. Compared with other tracking methods, the proposed method requires only one low-cost yaw rate sensor. The method utilizes electronic feedback from the phased-array antenna to compensate for the low-cost sensor irregularities. The effectiveness of the proposed tracking method is demonstrated by measured performance of a fast-moving ultra-low-profile phased-array satellite terminal, which uses the proposed approach. The field test results confirm that the hybrid tracking mechanism can nullify the base vehicle yaw disturbances up to $60^\circ/\mathrm{s}$ and $85^\circ/\mathrm{s}^2$ and keep the azimuth angle error at less than the permissible bound of $[-1^\circ, +1^\circ]$. Although performance of the proposed tracking system is verified in the context of a mobile satellite television reception system, the basic principles can be applied to any tracking system that employs phased-array antennas. The mobile satellite Internet terminal is an important example.**

***Index Terms*—Digital control system, direction-of-arrival (DOA) estimation, hybrid tracking, microelectromaechanical system (MEMS), real-time experiments, satellite communication system, sensor drift, tracking system.**

I. Introduction

THE DEMAND for mobile satellite broadcasting and communication has been growing rapidly for the past two decades [1]–[11]. To compensate for the considerable path loss from the satellite to the mobile end-users and achieve a desired signal-to-noise ratio, high-gain antennas with fast beam agility are required. However, to make the antenna system low profile without sacrificing radiation gain and vertical plane scanning range, the antenna beamwidth in azimuth should be significantly reduced. In a typical case, the azimuth beamwidth may have to become smaller than 1°. On the other hand, to deliver a high quality of service, the received signal level must be maintained above a predetermined threshold. This requires that the antenna beam be always pointed toward the satellite, with sufficient accuracy, during the platform maneuvers. Hence, the accurate tracking of the satellite is the essential requirement of the mobile satellite antenna systems. Real-time road tests reveal that the turning speed of a medium size car can be as fast as $60^\circ/\mathrm{s}$, with an angular acceleration of up to $85^\circ/\mathrm{s}^2$ (see Section VI and Fig. 15). The narrow beamwidth of the antennas makes the satellite tracking task during such fast maneuvers highly challenging.

A variety of satellite tracking methods, using the combination of a mechanical tracking and an electronic beam controlling, have appeared in the literature [1]–[8]. In [1], the monopulse method is adopted. Despite the accuracy of this method, it makes the entire system large and complicated. It needs four antenna units to accurately track the satellite in azimuth and elevation. Each of the four units requires separate downconverter. The system in [1] has a height of 35 cm and a weight of 50 kg and can only support one polarization. The conical scanning method is used in [2]–[4] to track the satellite signal. Tracking function is performed by using both the gyro data and the received satellite signal level. This technique results in a 1–2-dB signal loss and reduces the tracking speed considerably. The squint beam tracking technique is applied for phased-array antenna systems in [5]–[8]. Jeon *et al.* [5] use 1-D electronic beam scanning in elevation and mechanical scanning in azimuth. Two levels of phase shifters are used to form the main beam as well as the squint beam. The squint beam rotates around the main beam by adding an extra phase to the main level phase shifters. A similar tracking technique has recently been applied for broadband and direct broadcast services in a triband (i.e., Ka, K, and Ku) compact offset reflector [8]. However, the squint beam technique requires a complex and expensive extra level of phase shifters and needs a time-consuming calibration process. In addition, the above tracking methods usually require the following two sensors for azimuth tracking: 1) a yaw rate gyro and 2) an additional magnetic compass [8] (or an optical encoder [2]). Furthermore, to the best knowledge of the authors, the effectiveness of the aforementioned tracking systems in the presence of the base

Manuscript received July 7, 2008; revised October 16, 2008. First published January 6, 2009; current version published May 29, 2009. This work was supported in part by Intelwaves Technologies Ltd., by the Ontario Centre of Excellence, by the National Science and Engineering Research Council of Canada, and by Research In Motion. The review of this paper was coordinated by Prof. Z. Yun.

H. Bolandhemmat is with the Department of Mechanical and Mechatronics Engineering, University of Waterloo, Waterloo, ON N2L 3G1, Canada, and also with Intelwaves Technologies Ltd., Waterloo, ON N2L 6J2, Canada.

M. Fakharzadeh is with Intelwaves Technologies Ltd., Waterloo, ON N2L 6J2, Canada, and also with the Department of Electrical and Computer Engineering, University of Waterloo, Waterloo, ON N2L 3G1, Canada.

P. Mousavi is with Intelwaves Technologies Ltd., Waterloo, ON N2L 6J2, Canada (e-mail: Pmousavi@intelwaves.com).

S. H. Jamali is with the Department of Electrical and Computer Engineering, University of Tehran, Tehran 14156, Iran, the Department of Electrical and Computer Engineering, University of Waterloo, Waterloo, ON N2L 3G1, Canada, and Intelwaves Technologies Ltd., Waterloo, ON N2L 6J2, Canada.

G. Z. Rafi and S. Safavi-Naeini are the Department of Electrical and Computer Engineering, University of Waterloo, Waterloo, ON N2L 3G1, Canada.

Color versions of one or more of the figures in this paper are available online at http://ieeexplore.ieee.org.

Digital Object Identifier 10.1109/TVT.2008.2012159

vehicle strong yaw disturbances (i.e., $> 30^\circ/\mathrm{s}$ and $40^\circ/\mathrm{s}^2$) has yet to be investigated.

In this paper, a novel hybrid tracking technique for phased-array antenna systems is introduced. The proposed tracking technique combines the inertial yaw rate sensor data with the electronic feedback from the phased-array antenna to keep its extremely narrow beam accurately pointed toward the desired satellite. It comprises the following two embedded control mechanisms: 1) a mechanical stabilization loop and 2) an electronic beamformer that uses a direction-of-arrival (DOA) estimation algorithm. The stabilization loop is mostly responsible for counteracting the vehicle's sharp maneuvers. The low-cost microelectromaechanical system (MEMS) gyro, which is mounted on the antenna platform, provides most of the information required by this loop. The electronic beamforming tracks satellite signal and generates the receive beam. At the same time, the DOA algorithm uses the data available from electronic beamforming to compensate the sensor irregularities at no extra hardware cost. It aids the stabilization loop and eliminates the residual azimuth angle error.

As compared with other existing methods, the advantages of the proposed hybrid tracking scheme are given as follows: 1) It only requires one low-cost MEMS gyro; 2) whereas the squint beam technique utilizes two-layer phase shifters, the proposed method uses only one layer of low-cost analog phase shifters, which create a beam that carries out both tracking and receiving; 3) there is almost no tracking loss, as compared with the conical scanning and squint beam techniques, due to the fact that the peak of the main beam in the proposed method is always pointed toward the satellite; 4) in contrast to multichannel configuration in the complex and expensive monopulse method, the present method uses only a single channel downconverter; 5) it eliminates antenna platform chattering, which is inevitable in the other tracking techniques like the conical scanning method. As a result, the mechanical noise and fatigue are significantly decreased, leading to enhanced system lifetime and reliability. Furthermore, the proposed system is able to nullify vehicles' strong yaw disturbances (up to $60^\circ/\mathrm{s}$ and $85^\circ/\mathrm{s}^2$).

As mentioned above, the proposed technique aims at using only one low-cost sensor, such as a miniature MEMS yaw rate gyro. This raises serious challenges. The tracking mechanism ought to significantly rely on the inertial turn rate sensor as the only source of the vehicle motion information. Performance of low-cost MEMS sensors is degraded enormously by high rate drift and random noise. Moreover, sensor behavior varies with the ambient temperature changes.

The other challenge stems from the fact that to minimize the cost and complexity, the proposed system architecture also uses low-cost analog phase shifters. The characteristics of these devices depend on the environmental conditions, temperature, and humidity, as well as aging. As a result, implementation of the beamforming strategies that require prior knowledge of the phase-voltage characteristics is extremely difficult. These make the overall design of tracking algorithm a challenging task, which will be addressed in this paper.

In Section II, we present the configuration of a prototype phased-array antenna system that has been developed to experimentally verify the robustness and performance of the proposed method. In Section III, the tracking requirements are elaborated. Section IV deals with the mechanical stabilization loop using a single MEMS gyro. Section V describes the DOA estimation algorithm. The effectiveness of the proposed hybrid tracking system is confirmed through various field tests, which are given in Section VI. Finally, Section VII concludes the paper.

II. Antenna System Structure

The novel hybrid tracking algorithm, which will be elaborated in this paper, is implemented in an ultra-low-profile stair-planar phased-array antenna system for mobile broadcast satellite reception in the Ku band. The overall antenna height, including the radome, is only 6 cm, and the system has a 2-D electronic scanning capability. A detailed description of the system and its components can be found in [12]. It should be mentioned that although the following description refers primarily to the particular implementation of the proposed tracking method in this specific phased-array system, the basic principles can be applied to any tracking application that employs phased-array antennas.

This low-profile phased-array antenna comprises 17 subarrays for right-hand circular polarization (RHCP) and 17 subarrays for left hand circular polarization (LHCP) [see Fig. 1(a)]. In total, for each polarization, 496 microstrip elements have been used to provide a radiation gain of 31.5 dBi at a frequency band between 12.2 and 12.7 GHz with an axial ratio that is better than 1.8 dB. The antennas for each polarization are placed in five consecutive panels. Each panel holds three or four 2×8 and 2×16 microstrip subarray antennas that form a nonuniform array. The half power beamwidth (HPBW) in elevation is approximately $\pm 20^\circ$ for both 2×8 and 2×16 subarrays, and the azimuth HPBWs are $\pm 4.6^\circ$ and $\pm 2.8^\circ$ for the 2×8 and 2×16 subarrays, respectively [12]. Using the radiation characteristics of 2×8 and 2×16 subarrays, the total radiation of the whole array is computed and is shown in Fig. 2. Fig. 2(a) shows the elevation pattern when the panels are at 30° [see θ_{rot} in Fig. 1(a)]. The elevation patterns for different target locations around 30° are also included in this figure. Due to the wide pattern in the elevation plane, the maximum radiation gain drop is less than 0.7 dB for a target movement of $\pm 10^\circ$ in elevation. In contrast, Fig. 2(b) shows that the tolerance for the target movement around the azimuth angle is much less. The HPBW of the phased-array antenna without scanning is about 0.8° in azimuth. For the target location fixed at 90° at azimuth, the target can move around $\pm 2^\circ$ with a 2-dB scanning loss. To maintain a scanning loss less than 1 dB for better signal reception in all weather conditions, the electronic scan should be limited to $\pm 1^\circ$. This implies that the system needs more stringent beam control in azimuth than in elevation.

A general block diagram of the system is depicted in Fig. 1(b). Each subarray is connected to a voltage-controlled analog phase shifter via a low-noise amplifier (LNA) and cable, and for each polarization, the outputs of the 17 phase shifters are combined by a power combiner and then downconverted to an intermediate frequency by a low-noise block (LNB) module.

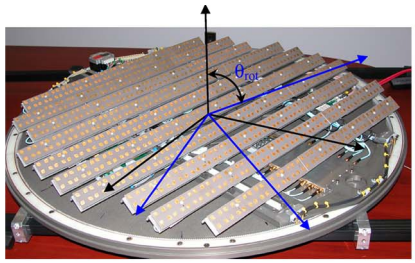

(a)

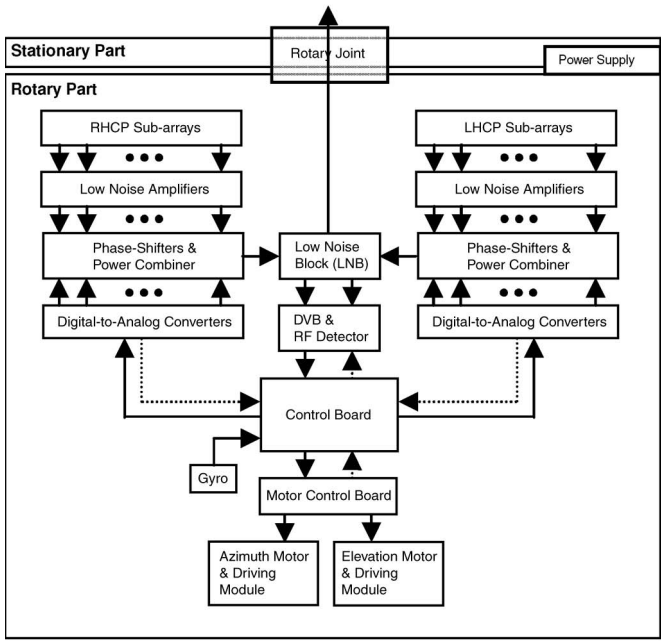

(b)

(c)

Fig. 1. Block diagram of the stair phased-array antenna system. (a) Phased-array antenna. (b) System configuration. (c) Phased-array antenna mounted on a car.

The output of the LNB is then divided into two parts. One goes to the satellite receiver via a rotary joint, and the other goes to the digital video broadcast (DVB) board and the radio-frequency (RF) detector. The task of the DVB board is to extract the satellite Identification (ID) for initial acquisition. The output of the RF detector is sampled and is then converted to digital signals. Based on the digitized RF level and the gyro information, the tracking algorithm implemented in a digital signal processor (DSP) on the main control board adjusts the

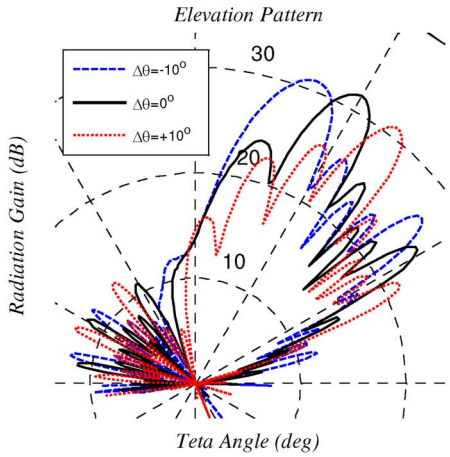

(a)

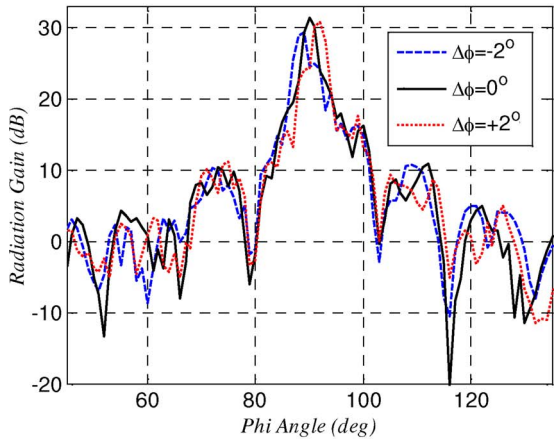

(b)

Fig. 2. (a) Radiation pattern of the phased-array antenna in the elevation plane for three different target locations. The mechanical angle of the antenna is fixed at 30°. (b) Radiation pattern of the phased-array antenna in the azimuth plane for three different target locations. The mechanical angle of the antenna is fixed at 90°.

phase shifter voltages and sends the required commands to the azimuth and elevation motors via motor control and motor driver boards.

All the aforementioned electronic parts, including the motors, are integrated in the antenna's rotating platform. An azimuth rotor assembly engages the rotating platform with the stationary part either through gears or a drive wheel attached to the azimuth motor. The systems with gears offer higher tracking accuracy, while those with wheels create less mechanical noise. However, the tracking accuracy of the systems with wheels can be enhanced by incorporating a spring-loaded mechanism that helps eliminate slippage of the drive wheel on the stationary drive ring.

The function of the antenna main control algorithm is to initially direct the antenna beam toward the desired satellite and then maintain a permanent beam pointing while the vehicle moves. In this regard, the control task can be divided into two modes, i.e., 1) an *initial satellite search mode* and 2) a *tracking mode* [12]. A *reinitialization mode* can also be foreseen for the cases when the satellite signal is lost for a period of time due to blockage or signal shadowing, and an initial search is required to retain the lock. In the tracking mode, the following two complementary mechanisms operate simultaneously: 1) the

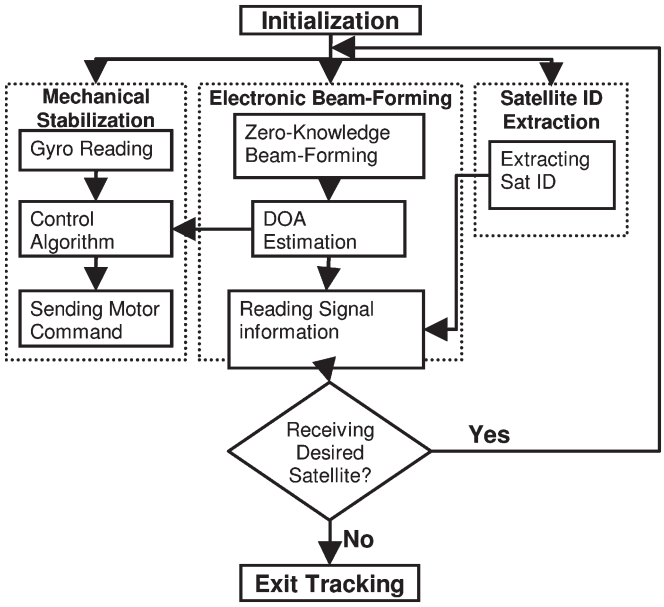

Fig. 3. Flowchart of the hybrid tracking mechanism.

stabilization loop and 2) a *DOA estimation algorithm based on electronic beamforming* (see Fig. 3). Section III lists the tracking system requirements.

III. Tracking System Criteria

The tracking algorithm shall steer the direction of the antenna toward a particular satellite while the base vehicle is roaming around. In general, the elevation beamwidth of a mobile low-profile antenna is considerably wider than the azimuth. This is due to the fact that the antenna aperture width in elevation is narrower than the antenna aperture length in azimuth. On the other hand, the electronic beam steering allows even larger coverage in elevation (in this case $\pm 20^\circ$). These compensate for the typical pitch and roll variations of the vehicle. Therefore, the hybrid tracking is performed only in the azimuth direction; while in elevation, the electronic beamforming compensate the vehicle movements. When the vehicle experiences a significant elevation angle changes (larger than electronic scanning capability in elevation), the antenna panels are mechanically rotated toward the satellite. Since the elevation change is a slow process (our measurements demonstrated that the elevation angular velocity is less than $10^\circ/\mathrm{s}$ [27]) compared with the azimuth, the beamforming algorithm has enough time to provide the required data.

The tracking system reacts in response to angular velocity disturbances caused by the vehicle movements. The disturbances are sensed by the inertial yaw rate sensor mounted on the antenna rotary platform. Since the HPBW of the antennas pattern is narrow (usually less than 1° in azimuth), the tracking mechanism should be fast and accurate enough to counteract the vehicle's sharp turns and hold the antenna at the prelocked bearing. Fig. 15 (see Section VI) plots the angular velocity and acceleration of the test vehicle measured during a harsh double-sided turn (S-shape) maneuver. It is apparent that the angular speed of the vehicle and its acceleration can exceed $60^\circ/\mathrm{s}$ and $85^\circ/\mathrm{s}^2$, respectively.

The tracking method relies significantly on the inertial turn rate sensor. However, performance of the sensor is degraded by the drift and random noise that can gradually divert the antenna's line-of-sight. The tracking system must be able to compensate for them to always keep the pointing error in the permissible bound of $[-1^\circ, +1^\circ]$ and to maintain a scanning loss less than 1 dB for better signal reception in all weather conditions. Furthermore, during passing behind an obstacle or going through a tunnel, when no aiding signal from the satellite is available, the tracking system must maintain the antenna beam correct direction only by the use of the gyro for at least 120 s.

The antenna system is also expected to remain functional in temperatures ranging from -30 °C to 60 °C. In such a wide temperature range, the gyro response has significant fluctuations. The tracking system must therefore be capable of handling the gyro characteristics variations.

IV. Stabilization Loop

The structure of the stabilization loop is described in this section. Each component of the loop is separately introduced and discussed. Step-by-step procedures are also given to select the modules. In addition, two novel filters are developed to reduce the effects of the low-cost MEMS gyro irregularities as well as its sensitivity to the ambient temperature changes. Section IV-B presents a practical and systematic methodology to design the loop digital controller such that the desired requirements are satisfied.

A. Stabilization Loop Structure

Fig. 4 shows the configuration of the antenna closed-loop stabilization mechanism. The yaw rate gyro measures the angular velocity of the antenna platform with respect to an inertial reference frame denoted by ω_{IA}. Once the acquisition process determined a predefined (target) satellite direction, the tracking system must hold ω_{IA} in the vicinity of zero to keep the antenna pointed at the satellite. The deviation of ω_{IA} from zero is the stabilizing loop error that enters the antenna computer hosting the tracking system's controller algorithm. By processing the error, an appropriate reaction to the latest angular velocity disturbance ω_d is then determined and sent as a command to the motor driver. The function of the motor is to rotate the antenna about the vehicle yaw axis by the desired magnitude and sign.

1) Motor: The motor should generate the required driving torque, which is a direct function of the required tracking acceleration α_t and the total moment of inertia of the antenna rotary components about the vertical axis I_{zz}. As pointed out, the motor must be capable of spinning the antenna platform with angular accelerations up to $85^\circ/\mathrm{s}^2$ ($\alpha_t \cong 1.5$ rad/s^2). Otherwise, the tracking cannot be performed properly causing the pointing error to grow beyond the allowable limits.

Considering the inertia of the rotating platform, the required torsional moment on the platform can be calculated from the Euler law ($T = I_{zz}\alpha_t$). The required torque on the motor shaft is then obtained by incorporating the driving gear or wheel ratio. However, the resistant torque by the Coulomb friction has yet to be taken into account. To allow for effects of the friction torque as well as uncertainties in the design process, the

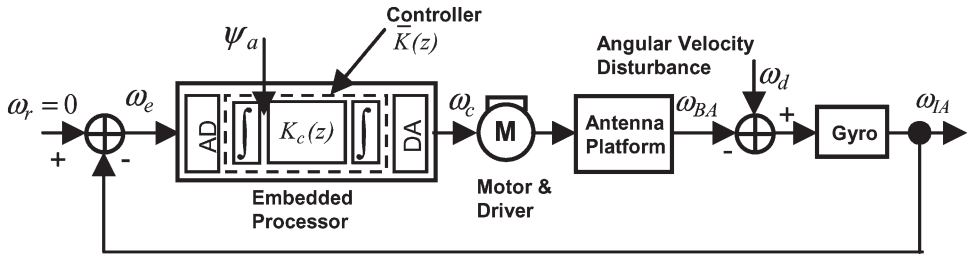

Fig. 4. Block diagram of the closed-loop stabilizing system.

calculated required torque on the motor head is multiplied by a safety factor (SF). The SF for the tracking system applications can be chosen between 3 and 7, depending on the power/torque transmission device that is being used. A factor of 3 can be considered for a wheeled torque transmission system, while a factor of 7 is more suitable for geared systems with higher friction torques.

Direct current (dc) motors are traditionally utilized in the tracking systems due to the relative ease of controlling them. This is mainly because of the fact that they demonstrate linear behaviors. However, there exist some disadvantages in using such motors for high-speed repetitive applications. Low life span (due to the brushes' weariness) and overheating of the armature windings are in that category [13]. In addition, the dc motors have a relatively low torque-to-inertia ratio (since the windings are on the rotor). As an alternative, the stepping motors can be employed for the tracking applications. Moreover, utilizing a stepping motor with a larger torque-to-inertia ratio compared with a same-size-class dc motor helps reduce the height of the mobile antenna systems.

2) Inertial Yaw Rate Sensor: Error budgets associated with the hybrid tracking systems usually fall in a region that allows for a gyro bias drift rate between $100^\circ/\text{h}$ and $400^\circ/\text{h}$ and scale factor stability of up to 700 ppm. Beyond that region, the hybrid tracking loop must be equipped with a fairly high sampling rate control system and external aid ($> 100-120$ Hz) to overcome the sensor drift. However, the challenge of maintaining the desired attitude during the aiding signal outages remains. A wide range of sensors from the high-precision ring laser gyros and the fiber optic gyros (wherein bias stability is not more than $150^\circ/\text{h}$) to the miniaturized silicon quartz gyros or the MEMS (wherein bias stability is up to $1000^\circ/\text{h}$) can afford the required performance [14]. However, the final sensor choice is usually made based on a tradeoff between cost, size, and accuracy.

Recent progress in the MEMS technology has led to the production of extremely low-cost inertial rate gyros [15]. Their small size combined with high durability and reliability makes them ideal for the commercial applications. However, these sensors suffer from an inherent high rate bias stability, high grade random noise, and relatively huge bias changes with temperature.

Fig. 5 depicts data captured from a typical low-cost MEMS gyro [16] when the antenna system is on a stand still for almost 120 s at 25 °C. The sensor noise represents an root mean square value of about $0.5^\circ/\text{s}$, which almost hides angular motions by as fast as $1.5^\circ/\text{s}$. The gyro bias stability is obtained using the Allen variance technique [17]. It is approximately $350^\circ/\text{h}$, which is close to the boundary. Furthermore, the rate random walk (RRW) of the sensor, which is calculated in the same fashion, is approximately $5000^\circ/\text{h}$.

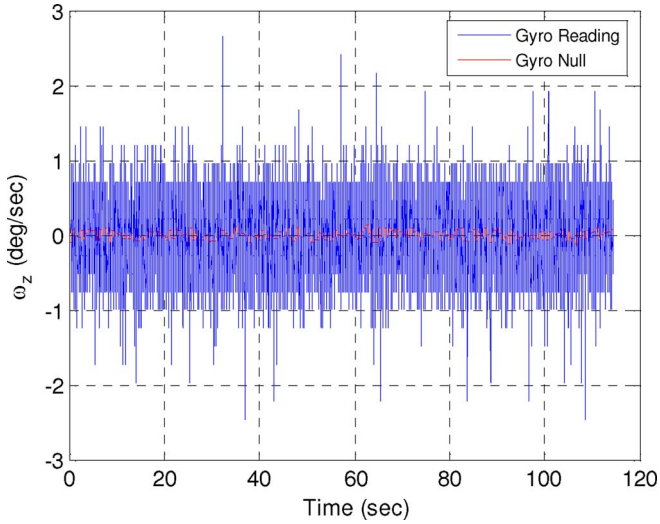

Fig. 5. Gyro readings and the corresponding null values when the antenna is at rest.

Although the selected gyro (or gyros in the same families) specifications are within the tolerable region designated for the tracking systems, preliminary real-time experiments confirmed that the antenna tracking system cannot rely on the gyro solely for more than 30 s (1σ) (the design requirement is 120 s). To achieve the required performance, the effect of the gyro drift and the random walk must be alleviated. Two cascade digital filters thereafter are devised and implemented, which are summarized in the following sections.

Gyro drift compensation: The first filter, consisting of a sliding average window, updates the gyro null value each τ_w milliseconds. The optimal width of the window is a function of the sensor bias stability and RRW and is determined by trial and error. In this case, τ_w is equal to 200 ms (5 Hz). The updated gyro null is then compared with a so-called base gyro null, which explicitly relates to the ambient temperature. Fig. 6 demonstrates the base gyro null trend with the ambient temperature variations obtained by the temperature chamber experiments. If the difference is less than a predefined threshold (between 0.15 and 0.45 least significant bit (LSB) based on τ_w), the up-to-date gyro null is used in the stabilization loop computations. Otherwise, the base gyro null is considered as the new bias (see Fig. 7). This procedure repeats faster (up to 100 Hz) at the beginning of the vehicle motion since the

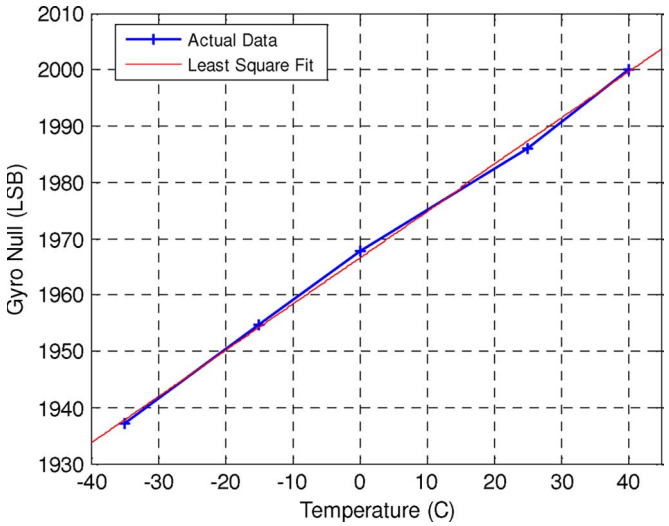

Fig. 6. Gyro null versus temperature.

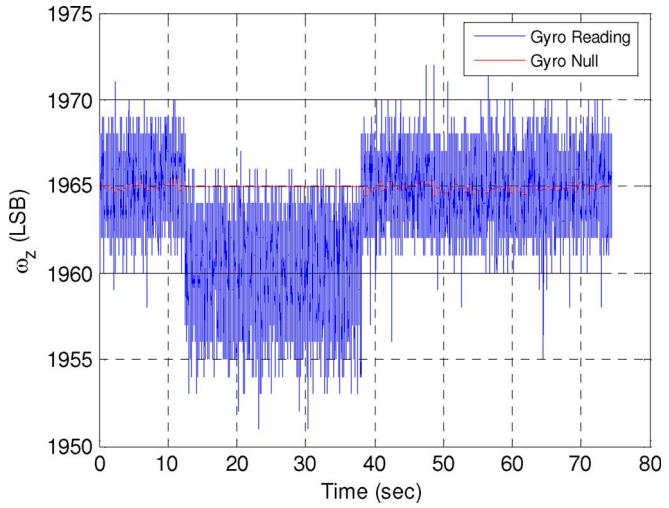

Fig. 7. Update process of the gyro null value. Data are presented in binary format.

sensor dice experience higher temperature changes when the antenna/tracking system is turned on.

The second filter compares the gyro data within the current window with some reference patterns (previously stored) to distinguish if the pointing error is a result of the gyro drift/random walk or a result of an actual movement of the vehicle. In the case of gyro fault, it resets the antenna's pointing error and triggers a flag for the stabilization loop requesting not to take any action. This way, the effects of the gyro irregularities are filtered out effectively and not transferred to the stabilization loop. This helps the tracking system to perform smoothly without any chattering around the desired azimuth angle. The outcome of this layer (the flag status) is also fed back to the first filter, serving as an additional decision making measure to update the gyro null. Hence, the sliding window contents of the moving vehicle (when the flag is off) is not considered in evaluating the gyro null. Fig. 8 illustrates the performance of the proposed filters. It is shown that the heading error due the gyro drift and noise is restricted to a narrow bound of $\pm 0.2^\circ$ for even more than 120 s.

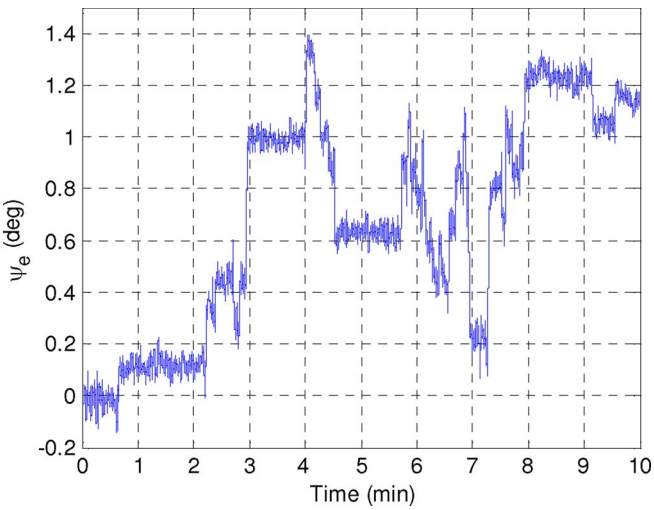

Fig. 8. Azimuth angle error caused by the gyro drift. The antenna stands still, and the motor is off.

3) Digital Controller: The digital control law $\bar{K}(z)$ is the kernel of the stabilization loop that is programmed on the on-board DSP (see Fig. 4). It is driven by the stabilizing loop error ω_e, which is the perturbed angular velocity of the antenna platform from the desired angular velocity, which is zero (i.e., $\omega_r = 0$). ω_e is measured by the gyro mounted on the rotating platform. By manipulating the stabilizing loop error, the controller $\bar{K}(z)$ produces suitable commands to the motor driver circuit to nullify the angular velocity disturbance. The controlled system response to the external disturbances is expected to be slightly underdamped with a maximum percent overshoot (MPOS) of around 10%–15%.

The bandwidth of the stabilization loop is determined based on the frequency content of the angular velocity disturbances ω_e (see Fig. 4). Fig. 9(a) portrays frequency components of a typical disturbance input exerted by the test vehicle [fast Fourier transformation (FFT) of the angular velocity curve in Fig. 15]. The graph demonstrates the energy distribution over the frequency domain. It is apparent that the dominant frequency components of the disturbance input concentrate on the frequencies less than 0.5 Hz. As a result, the controller must amplify the magnitude of the stabilization loop gain in these frequencies over nearly 25 dB (assuring a high loop gain in the designated frequencies [20]) to efficiently reject the external disturbances. However, there exist some minor frequency components above that range up to approximately 4.5 Hz. It is shown by the power spectral density (PSD) of the signal given in Fig. 9(b). Therefore, the bandwidth of the control system is rendered around 4.5 Hz ($\approx$30 rad/s) to guarantee the elimination of the effects of the angular velocity disturbances on the entire frequency range. It is obvious that the stabilization loop's required bandwidth may vary slightly, depending on the type of the base vehicle (car or boat or train). The digital controller design procedure is presented in Section IV-B.

B. Stabilization Loop Controller Design

As Fig. 4 illustrates, the stabilization loop controller design involves the specification of $\bar{K}(z)$ such that the aforementioned

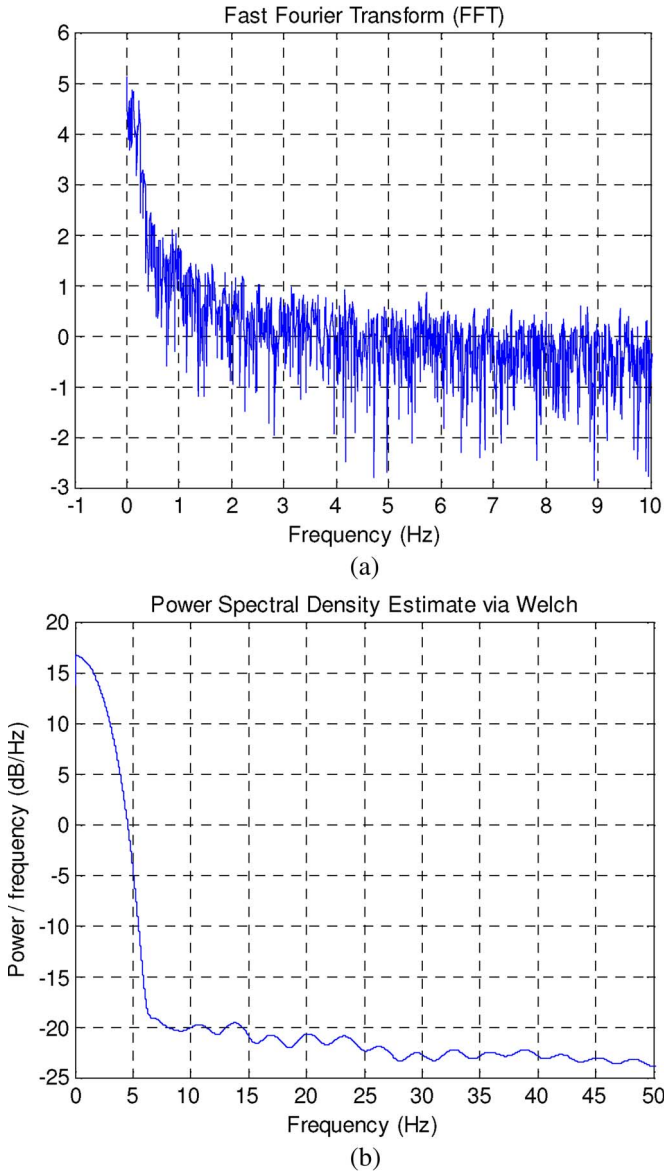

Fig. 9. (a) Spectrum of the base vehicle angular velocity disturbance depicted in Fig. 15. (b) PSD of the base vehicle angular velocity disturbance.

time and frequency domain requirements are satisfied. The design process begins with the mapping of the control problem into the w plane by the use of the bilinear transformation (i.e., the Tustin method) [20]. The design is then accomplished in the w plane. Finally, the designed controller is converted to the z domain via inverse mapping.

From the time domain requirements, input disturbances that have the form of either step or ramp should be asymptotically rejected. A sufficient condition for the disturbance compensation (with no steady-state error), referring to the internal model principle, is that the open-loop system must contain two similar poles at $z = 1$ (type 2 system). This is done by embedding two integrators in $\bar{K}(z)$, as shown in Fig. 4. Subsequently, the original controller design problem is altered to the design of an inner controller $K_C(z)$ (see Fig. 4) to satisfy the frequency domain specifications.

The first integrator output is the antenna's pointing error Ψ_a. The pointing error is the deviation of the antenna heading angle from the reference azimuth assigned by the initial acquisition mechanism. The response of the internal controller function to the pointing error of the antenna platform is an acceleration (torque) command. The acceleration order is then converted to a velocity command by the second integrator and is finally sent to the motor driver. The stepper motors have an extremely nonlinear dynamics [13], [18], [19]. However, in the angular velocity range of interest for the antenna tracking problems, a linear transfer function can reasonably describe behavior of the moving platform's angular velocity ω_{BA} (which drives by the stepper motor) in response to the following velocity command:

$$G(s) = \frac{\omega_{\mathrm{BA}}}{\omega_C} = \frac{1}{\tau_s s + 1}. \tag{1}$$

The time delay τ_s relates to the load inertia. It also reflects the existence of gear backlash/driving wheel slippage and Coulomb friction in the system. It is usually evaluated by experiments. For the present antenna system, it is approximately 10 ms $(\tau_s = 0.01)$ [since τ_s is evaluated to be fairly small, the antenna transfer function (1) might even be overlooked in the control system design].

Sampling frequency of the discrete control system is a function of the control loop bandwidth (usually five to ten times greater). For a bandwidth of about 4.5 Hz, a sampling rate of around 45 Hz avoids aliasing and allows perfect reconstruction of all loop signals. However, to enhance the accuracy of the numerical integrations in the forward path, the sampling frequency of the control loop is usually doubled (100 Hz for the present system).

Fig. 10(a) shows the frequency response of the control system loop gain, excluding the inner controller $K_C(z)$ in the w plane. With the high sampling frequency, the frequency warping through the bilinear transformation is negligible [20]. Hence, the desired crossover frequency ($\approx 80\%-85\%$ of the closed-loop bandwidth) in the z plane and the w plane remains almost identical.

Considering the bode plot of the open-loop gain [see Fig. 10(a)], the corresponding phase at the designated crossover frequency (nearly 25 rad/s) is obtained. It is approximately 160° in this case. Subsequently, the additional phase (about $70^\circ-80^\circ$) required to provide the desired transient response performance (MPOS $< 15\%$) is augmented by the use of a properly designed lead compensator of the form

$$K_C(w) = k_w \frac{w + w_z}{w + w_p}. \tag{2}$$

For the present system, the lead controller zero and pole are located at $w_z = 2.2$ and $w_p = 286$, respectively. The compensator gain k_w is then determined to shape the desired magnitude behavior at low frequencies (i.e., < 0.5 Hz). After setting k_w, mapping the w plane controller with the inverse Tustin [20] transformation yields the final discrete-time lead compensator, which is given by

$$K_C(z) = k_z \frac{z + z_z}{z + z_p}. \tag{3}$$

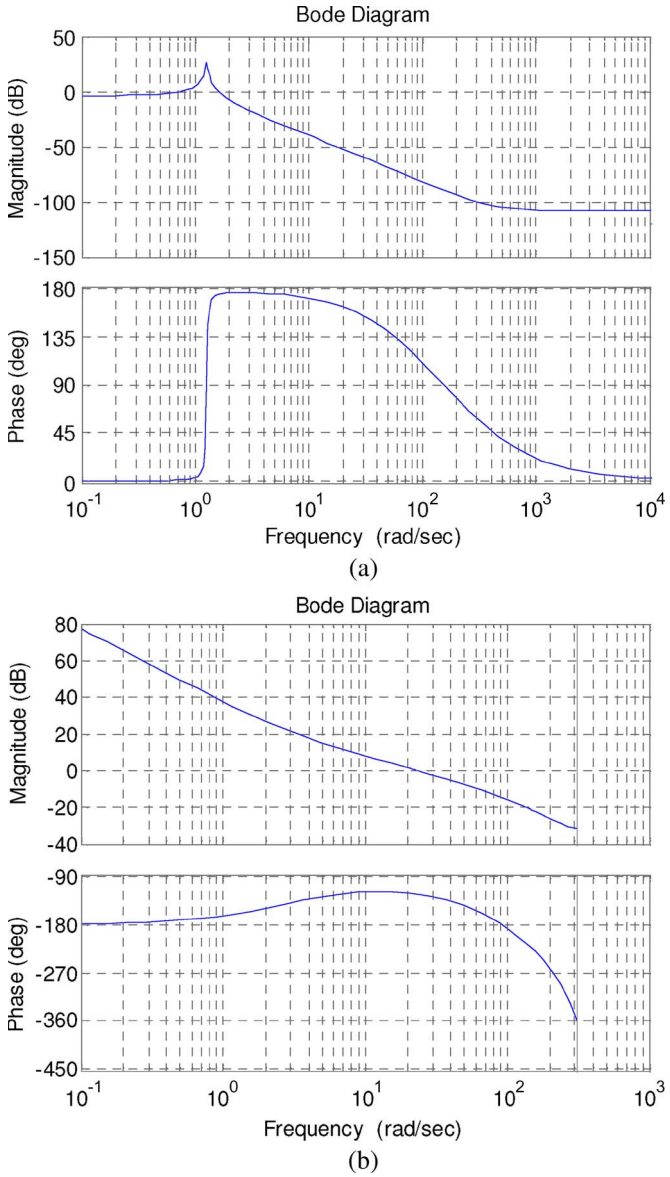

Fig. 10. (a) Bode plot of the open loop in the plane. (b) Open-loop frequency response of the digital control loop shown in Fig. 4.

The parameters of the ultimate lead controller for the present antenna system are $z_z = -0.97$, $z_p = 0.179$, and $k_z = 2912$. Fig. 10(b) shows the open-loop frequency response of the discrete control system (see Fig. 4), which also includes the lead compensator (3) influence. It is apparent that introducing the compensator results in a phase margin of about 60° (with a damping ratio of $\xi \approx 0.6$ or MPOS $\approx 10\%$) at the crossover frequency of approximately 25 rad/s. In addition, the behavior of the loop gain at the low frequencies has also been improved.

V. DOA Estimation Using Electronic Beamforming

The low-cost MEMS sensor employed in the stabilization loop suffers from the high rate drift and strong noise, which deflects the antenna heading from the desired direction. Moreover, some slow angular disturbances of the vehicle are even hidden in the sensor noise. As a result, the stabilizing loop takes no action to compensate for such disturbances that may cause complete signal loss. The DOA estimation algorithm uses received satellite signal to compensate for the low-cost sensor inaccuracies. It takes advantage of the exclusive property of the phased-array antenna to electronically steer the antenna beam; hence, there is no need to move the whole system permanently, which causes fluctuations (and power drop) in the received signal and reduces the mean life of motor [2]–[4]. The so-called zero-knowledge beamforming algorithm is applied to maximize the received signal power by setting proper phases for the phase shifters [11], [12], [27]. Meanwhile, by monitoring the control voltages of the phase shifters, the direction of the satellite relative to the array antenna is estimated.

Several algorithms have been proposed to estimate the DOA of an active source; among them, MUSIC [21], Capon [22], and ESPRIT [23] are frequently used. However, such methods need either full access to received signals from each antenna individually, which means that each antenna element must be followed by a full baseband receiver, or very accurate phase shifter characteristics should be known and used in the system [24]. The former increases the cost and the processing load, while the latter needs time-consuming laboratory measurements or accurate calibration to update the phase shifter characteristics. Some of the developed DOA estimation methods for single-receiver phased-array systems estimate the spatial covariance matrix of the received signals by perturbing the weights and use optimal weight theorems (e.g., Weiner filter). Such methods need $2(n^2+1)N$ perturbations, where n is the rank of the covariance matrix, and N is the number of antenna elements, which can be a huge number [25]. Moreover, the estimated covariance matrix is inaccurate and is sometimes ill-conditioned. It is well known that platform motions significantly affect the estimated covariance. Even a relatively small displacement of the source during the time required for covariance estimation causes a significant error and gain drop [26].

A novel DOA estimation method is introduced in the following. The algorithm is fast and accurate over a limited angular range. It does not add to the complexity of the system and eliminates the need to rotate the antenna platform permanently. The DOA estimation and beamforming algorithms [27] do not depend on the device characteristics, which may be affected by the ambient conditions and the system aging.

A. Functional Block Diagram

Fig. 11(a) demonstrates the functional block diagram of the DOA estimation algorithm. The beamforming algorithm adjusts the control voltages of the phase shifters $(V_1, \ldots, V_N)$ to maximize the received signal power. These voltages, along with the measured received power, are sent to the DOA estimation algorithm, which collaborates with a database to find the satellite direction with respect to the array. When the direction is found, a proper left or right command (L/R CMD) is sent to the motor to adjust the array direction.

B. Received Signals Model for an Array

To clarify the concept of DOA algorithm, first, the received signal model is described. Fig. 11(b) shows a simplified array of three elements; each element has been connected to a phase

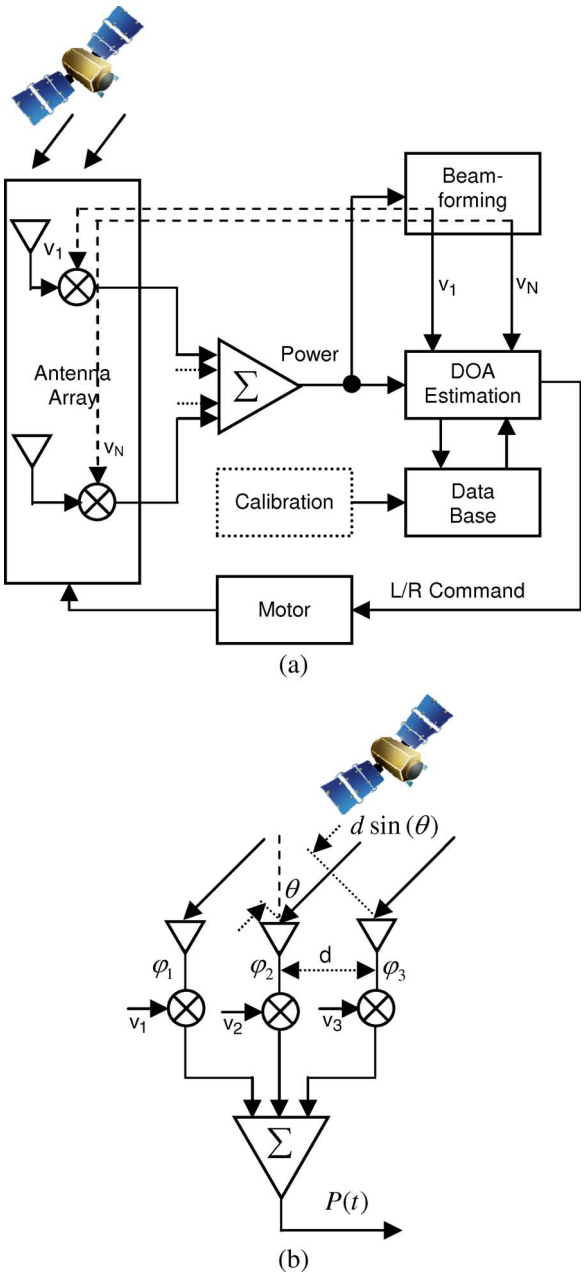

Fig. 11. (a) Functional block diagram of the DOA estimation algorithm. (b) Phased-array antenna with three elements.

shifter. Each phase shifter generates a phase shift corresponding to its control voltage, which is adjusted by the beamforming algorithm. These phase shifts are added to the signals coming from antennas, and all signals are combined by the power combiner Σ. The combined signal goes through a mixer and detector, where the total received power $P(t)$ is measured. This is the only available feedback from the satellite and is used as the input of the beamforming program to adjust the control voltages.

When the satellite direction is aligned with the array normal [see the dashed line in Fig. 11(b)] or $\theta = 0$, the highest power is obtained if all signals from arrays are coherently combined $(\varphi_1 = \varphi_2 = \varphi_3)$. This implies that all phase shifters must have the same control voltage (i.e., $V_1 = V_2 = V_3$) if their characteristics are identical. If the wave-front of the satellite signal makes angle θ with the array normal, there will be a

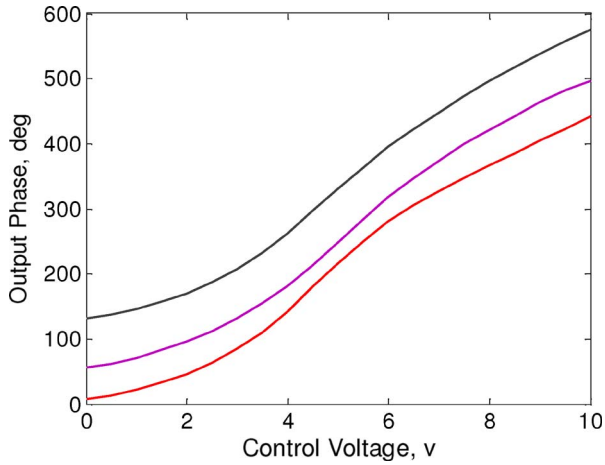

Fig. 12. Characteristics of the three channels of a phased-array antenna, including varactor-based phase shifters, LNAs, and cables. The input voltages change from 0 to 10 V and generate phase shifts more than 360°.

phase lag between the antenna elements. The phase lag between adjacent elements is related to the spacing d, wavelength λ, and DOA θ by

$$\varphi_1 - \varphi_2 = \varphi_2 - \varphi_3 = \frac{2\pi d}{\lambda}\sin(\theta). \tag{4}$$

In the present phased-array antenna system, $d = 223$ mm, and $\lambda = 24$ mm. If the satellite moves 1° to the right (clockwise direction), the phase difference between the adjacent elements becomes $\Delta\varphi = 58.4^\circ$. This is a fairly large phase difference, however, we do not have access to the signal phase. The only thing that we can control is the input voltage of the phase shifters. If all phase shifters were identical with a linear relation between phase and control voltage (i.e., $V = K_0\varphi$), then

$$V_1 - V_2 = K_0\frac{2\pi d}{\lambda}\sin(\theta) \tag{5}$$

which means that by comparing the adjacent voltages, the satellite's DOA can be found, i.e.,

$$\theta = \sin^{-1}\left[\frac{\lambda\Delta V}{K_0 2\pi d}\right] \tag{6}$$

where $\Delta V = V_1 - V_2 = V_2 - V_3$. However, practically, the assumptions of having identical phase shifters and a linear $V-\varphi$ relation are not valid. Fig. 12 shows the characteristics of the three channels of a phased array consisting of varactor-based analog phase shifters, LNAs, and cables used in this system. The curves are not identical, but they show similar behaviors. For example, there is a monotonic relation between phase and voltage of the phase shifters; however, such phase–voltage relations are not linear, and they are subject to change due to the environmental conditions and aging [11].

C. Beamforming Algorithm

The goal of beamforming is to compensate the interelement phase lags by adding proper phase shifts to maximize the total received power. To this end, we have introduced the zero-knowledge beamforming algorithm [11], [27], in which the

control voltages of all phase shifters are sequentially perturbed to estimate the gradient of power relative to voltages and update the control voltages. This algorithm is suitable for mobile scenarios and can steer the array beam toward the satellite as long as the satellite signal is the dominant received signal. As the satellite moves relative to the array axis, the control voltages are adjusted.

Let $\mathbf{v}(n) = [V_1(n) \quad V_2(n) \quad \cdots \quad V_N(n)]$ denotes the vector of the control voltages applied at time instant n. According to the zero-knowledge beamforming algorithm [27] the new set of voltages $\mathbf{v}(n+1)$ can be calculated (updates) as

$$\mathbf{v}(n+1) = \mathbf{v}(n) + 2\mu\hat{\mathbf{G}}(n) \tag{7}$$

where μ is the step size, and $\hat{\mathbf{G}}(n) = [\hat{g}_1(n) \quad \hat{g}_2(n) \quad \cdots \quad \hat{g}_N(n)]$ is the estimated gradient vector. Each element of the gradient vector is calculated using a centered difference approximation as

$$\hat{g}_i = \frac{P(V_1, \ldots, V_1+\delta, \ldots + V_N) - P(V_1, \ldots, V_1-\delta, \ldots + V_N)}{2\delta} \tag{8}$$

where δ is the perturbation in the phase shifter control voltages. Equations (7) and (8) constitute the core of the beamforming algorithm for a satellite receiver [27].

D. DOA Estimation Algorithm

The beamforming algorithm finds the voltages that maximize the received power. As shown in Fig. 11(a), the proposed DOA estimation algorithm uses these voltages, the measured power, and the information of the database. From Fig. 12, it is understood that (6) cannot be used to estimate the satellites' direction from the control voltages. One way to overcome this disadvantage is to find a reference voltage for each phase shifter, i.e., $V_{\mathrm{Ref}1}, V_{\mathrm{Ref}2}$, and $V_{\mathrm{Ref}3}$. The reference voltages are those corresponding to a perfect pointing situation where the geometrical axis of the antenna array is accurately directed toward the satellite and phase voltages have a stable value. Hence, instead of comparing the absolute value of control voltages, one can compare their differences with their references, i.e., $\Delta V_i = V_i - V_{\mathrm{Ref}i}$. A simple training test, which can be a part of the calibration process in Fig. 11(a), can be run during the last step of satellite acquisition phase to find the reference voltages. During the training test, the phased-array antenna is mechanically rotated around the satellite direction in fine angular steps. The electronic beamforming is performed for each mechanical step, and the received power level and the final control voltages are recorded. At the end of this calibration process, the control voltages that result in the highest power level are reported as the reference voltages to the DOA algorithm, i.e.,

$$V_{\mathrm{Ref}i} = V_i(\theta_0)|_{P(\theta_0)=P_{\max}}. \tag{9}$$

Fig. 13 shows the result of a training test to find the reference voltages. The control voltage of the middle element V_{mid} is fixed (at 6.1 V in this case). The array is moved to -2.1° of the satellite direction and then rotated in 15 angular steps to cover

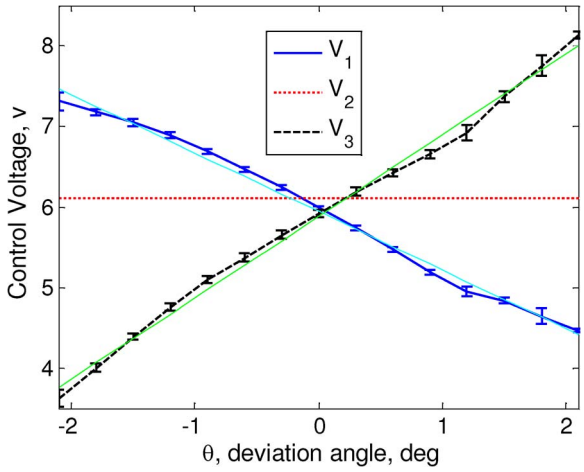

Fig. 13. Result of the calibration test for finding the reference voltages.

$\pm 2.1^\circ$ in azimuth. For each step, the beamforming algorithm is run m times to cancel the noise effect, and the final voltages are recorded ($m = 50$ in this case). The error bars show the standard deviation of the recorded values. The values of V_1 and V_3 at $\theta = 0^\circ$ are the reference voltages $V_{\mathrm{Ref}1}$ and $V_{\mathrm{Ref}3}$. Since the phase shifters are not identical, the cross point voltage is different from V_{mid}. The slope of V_1 is negative in accordance to (4)–(6). The reverse is true for V_3.

Once the reference voltages are found, the difference voltages ΔV_i are formed and compared with a voltage margin V_{Mar} to find the DOA. A voltage margin is necessary because of the existence of noise and disturbance during the beamforming process. Based on the results, as shown in Fig. 13, for the three-element array [see Fig. 11(b)], the following rules can be extracted.

1) If the target (satellite in this case) is on the right side of the array normal, we must have

$$\begin{cases} \Delta V_1 > V_{\mathrm{Mar}} \\ \Delta V_3 < -V_{\mathrm{Mar}}. \end{cases} \tag{10}$$

2) If the target is on the left side of the array normal, then

$$\begin{cases} \Delta V_3 > V_{\mathrm{Mar}} \\ \Delta V_1 < -V_{\mathrm{Mar}}. \end{cases} \tag{11}$$

3) Otherwise, the target is along the array normal, i.e.,

$$\left(-V_{\mathrm{Mar}} < \begin{cases} \Delta V_1 \\ \Delta V_2 \end{cases} < V_{\mathrm{Mar}}\right).$$

Based on the above rules, the DOA estimation algorithm is implemented. After running the training test, the reference voltage of each element and the maximum received power $P_{\max}$ are stored in the database. The received power level $P(t)$ is continuously monitored, and if it drops below a threshold, i.e., $P(t) < \gamma P_{\max}$, $\gamma < 1$, which is determined by the quality of the baseband signal, then the beamforming algorithm starts to update the voltages. If an increase in the power level is observed, the DOA algorithm starts comparing the current voltages with the references and determines whether the satellite is on the left side or the right side of the array normal and sends the proper

command (L/R CMD) to the stepper motor. A lower bound for the voltage margin in (10) and (11) is $V_{\mathrm{Mar}} \geq 2\sigma_{\max}$, where $\sigma_{\max}$ is the standard deviation of the received signal noise. During this process, if the measured output power exceeds the recorded value for $P_{\max}$, i.e., $P(t) > P_{\max}$, the database is updated, and the current voltages replace the reference voltages. If there are N rules for DOA estimation, then the algorithm needs N add/subtraction (to form the difference voltages) and $2N$ comparisons [as in (10) or (11)] to apply each rule.

As demonstrated above, the DOA estimation algorithm uses the received satellite signal to fine-tune the antenna's direction that deviated from the desired attitude due to the sensor inaccuracies. In other words, the DOA algorithm eliminates the effects of the sensor irregularities. Consequently, the hybrid tracking system with the DOA estimation algorithm resembles a stabilization loop (Fig. 4) whose inertial sensor has no deficiency (no drift and noise). Asymptotic stability and the required performance of such a stabilization loop with an ideal inertial sensor (i.e., $G_{\mathrm{gyro}} = 1$) is guaranteed through the design procedure of Section IV. Section VI investigates the effectiveness of the integrated tracking system by field experiments on a low-profile phased-array antenna system.

VI. Real-Time Experiments on the Hybrid Tracking System

A. Experiment Apparatus

The phased-array antenna system is mounted on the roof of a test vehicle, as shown in Fig. 1(c). The system variables are monitored and registered by a computer. The output of the antenna system is connected to a satellite television, and its strength is evaluated by the RF detector implemented in the antenna system. The vehicle yaw rate is measured by an additional gyro installed on the antenna base (stationary part of the antenna system with respect to the vehicle body). The tests are conducted in Waterloo, ON, Canada, with an elevation angle of around 35°. The target satellite was the Bell Expressvu 91.

The following tasks are implemented in three different threads running on the antenna DSP: 1) the stabilization loop; 2) the electronic beamforming; and 3) the satellite ID extraction (see Fig. 3). The satellite ID is extracted by a DVB chip from the received signal. The beamforming process continuously updates the control voltages of the phase shifters to maximize the received signal power. At the same time, it estimates the DOA and sends this information to the antenna control unit. Based on the DOA estimates and the yaw rate sensor data, the hybrid tracking algorithm provides the stepper motor with proper commands to point the beam always toward the target satellite.

B. DOA Estimation: Experimental Results

As discussed in Section II, there are 17 elements in the whole phased-array system. Five of these elements are approximately located on the symmetry axis and the variation of the required phase-shift is negligible for them; therefore, at most 12 rules similar to (10) and (11) can be defined for this system. Defining more rules lowers the error probability in the DOA estimation.

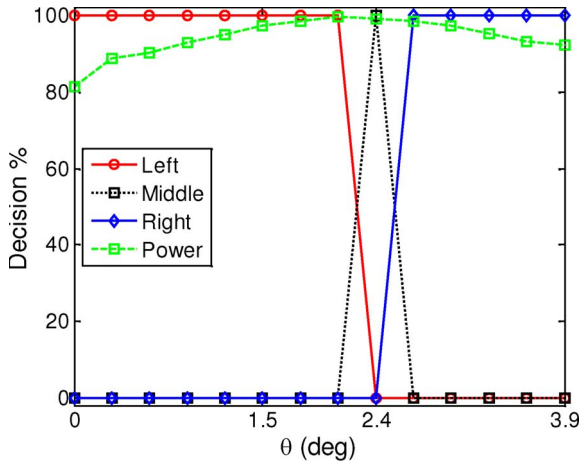

Fig. 14. Experimental results for DOA estimation.

Fig. 14 shows the results of an off-board test. The test procedure is given as follows. Once the satellite was found (end of acquisition phase) and the reference voltages were stored in the database, the array was moved randomly to a position to the left of the satellite denoted by $\theta = 0$ in Fig. 14. The beamforming and DOA algorithms were run, and the relative direction of the satellite was found correctly. This process was repeated numerous times to find the error probability, and in all runs, the same result was obtained. L/R command was disabled for the test purpose, and therefore, the array was manually rotated to the right side in steps of 0.3°. As shown in Fig. 14, the DOA algorithm announces the satellite position (labeled as middle) at $\theta = 2.4°$ relative to the start position. Accordingly, at the same position, the received power peaks. The array is rotated for a few more steps to check the performance of the algorithm when the array is on the right side of the satellite. For all positions, the performance of the DOA estimation algorithm is completely satisfactory.

C. Road Test Results

Fig. 15 illustrates the yaw rate of the test vehicle (the angular velocity disturbance) and the associated angular acceleration in a sharp fishhook maneuver. During the maneuver, the antenna system experiences a maximum angular velocity of about $60°/\mathrm{s}$. The maximum angular acceleration also reaches $85°/\mathrm{s}^2$. Fig. 15 illustrates how such a sharp angular velocity disturbance can be efficiently nullified by the tracking system. It is apparent that the antenna pointing error always remains in the permissible bound of $[-1°, +1°]$.

Fig. 16 exhibits the yaw rate of the test vehicle in a complex multimaneuver experiment. At the beginning, the vehicle is at rest for more than 130 s. The embedded filters described in Section IV-A-2-a diminish the effects of the gyro drift for almost 100 s such that no correction is needed. After that, the DOA algorithm intervenes to cancel out the drift and fine-tune the antenna direction. As Fig. 16 demonstrates, by incorporating the embedded filters, the supervisory DOA algorithm is required to fine-tune the antenna direction almost each 10 s (0.1 Hz, 1σ value, which is about ten times slower than the existing techniques). As a result, the mechanical noise and

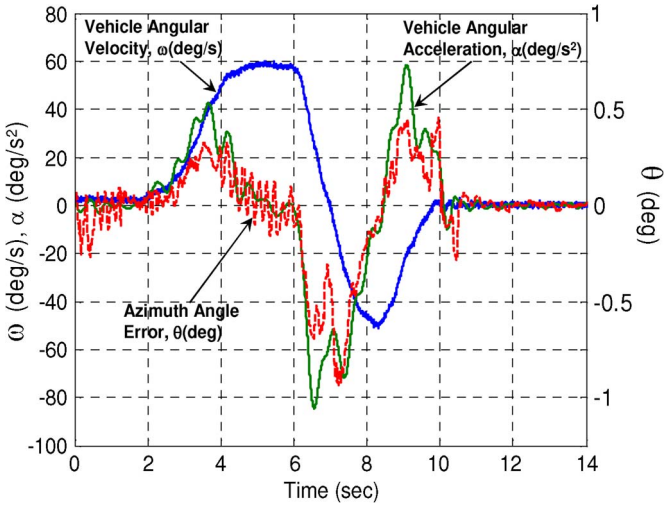

Fig. 15. Yaw rate of the test vehicle and the associated angular acceleration and azimuth error of the antenna platform due to this disturbance.

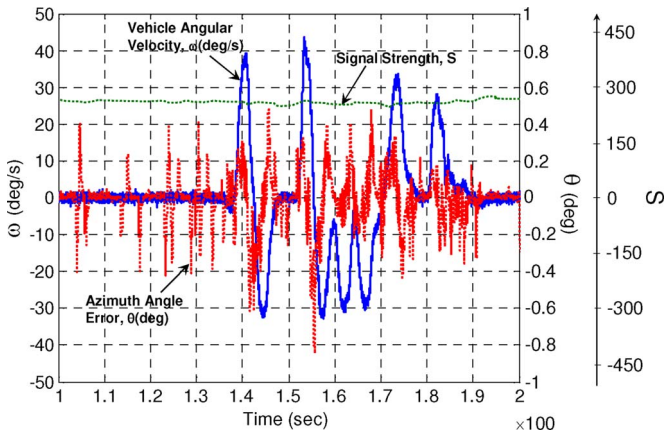

Fig. 16. Yaw rate of the test vehicle and the corresponding output power in a multiscenario maneuver and the antenna's heading error, which is the result of this angular disturbance.

vibration is significantly reduced. The effectiveness of the hybrid tracking system is also illustrated after $t \approx 140$ s when the vehicle turns are started. This time, the antenna system experiences angular velocities and accelerations up to $45^\circ/\mathrm{s}$ and $75^\circ/\mathrm{s}^2$. Both the antenna's pointing error plot and the received satellite signal confirm that the tracking task is performed flawlessly. It is apparent that the antenna's azimuth error is always in the permissible region (i.e., $[-1^\circ, +1^\circ]$), and therefore, the RF signal level remains almost constant.

VII. Conclusion

A novel hybrid tracking method for mobile active phased-array antenna systems was developed and successfully tested on an ultra-low-profile phased-array antenna for a land-mobile satellite receiver. The proposed method consisted of a stabilization loop and a DOA estimation algorithm that is based on electronic beamforming. The combined tracking system allowed for the use of only one low-cost yaw rate sensor as well as low-cost analog phase shifters. The field test results show that the hybrid tracking system can nullify the vehicle yaw disturbances up to $60^\circ/\mathrm{s}$ and $85^\circ/\mathrm{s}^2$ and keep the azimuth angle error less than the permissible bound of $[-1^\circ, +1^\circ]$. The built-in adaptability in the proposed hybrid tracking method makes it immune to environmental changes, such as temperature and humidity, as well as aging.

Acknowledgment

The authors would like to thank M. Hossu and Dr. K. Narimani for providing the test setup.

References

[1] Y. Ito and S. Yamazaki, "A mobile 12 GHz DBS television receiving system," *IEEE Trans. Broadcast.*, vol. 35, no. 1, pp. 56–62, Mar. 1989.
[2] A. C. Densmore and V. Jamnejad, "A satellite-tracking K- and Ka-band mobile vehicle antenna system," *IEEE Trans. Veh. Technol.*, vol. 42, no. 4, pp. 502–513, Nov. 1993.
[3] T. Wantanabe, M. Ogawa, K. Nishikawa, T. Harada, E. Teramoto, and M. Morita, "Mobile antenna system for direct broadcasting satellite," in *Proc. IEEE Int. Symp. Antennas Propag.*, Jul. 21–26, 1996, vol. 1, pp. 70–73.
[4] J. Hirokawa, M. Ando, and N. Goto, "A single-layer slotted leaky waveguide array antenna for mobile reception of direct broadcast from satellite," *IEEE Trans. Veh. Technol.*, vol. 44, no. 4, pp. 749–755, Nov. 1995.
[5] S. Jeon, Y. Kim, and D. Oh, "A new active phased array antenna for mobile direct broadcasting satellite reception," *IEEE Trans. Broadcast.*, vol. 46, no. 1, pp. 34–40, Mar. 2000.
[6] S. H. Son, S. Y. Eom, and S. I. Jeon, "A novel tracking control realization of phased array antenna for mobile satellite communications," in *Proc. 57th IEEE Semiannual VTC—Spring*, Apr. 22–25, 2003, vol. 4, pp. 2305–2308.
[7] U. H. Park, H. S. Noh, S. H. Son, K. H. Lee, and S. I. Jeon, "A novel mobile antenna for Ku-band satellite communications," *ETRI J.*, vol. 27, no. 3, pp. 243–249, Jun. 2005.
[8] S. Y. Eom, S. H. Son, Y. B. Jung, S. I. Jeon, S. A. Ganin, A. G. Shubov, A. K. Tobolev, and A. V. Shishlov, "Design and test of a mobile antenna system with tri-band operation for broadband satellite communications and DBS reception," *IEEE Trans. Antennas Propag.*, vol. 55, no. 11, pp. 3123–3133, Nov. 2007.
[9] C. D. Mccarrick, "Offset stacked patch antenna and method," U.S. Patent 7 102 571, Sep. 5, 2006.
[10] I. Stoyanov, V. Boyanov, B. Marinov, Z. Dergachev, and A. Toshev, "Mobile antenna system for satellite communications," U.S. Patent 6 999 036, Feb. 14, 2006.
[11] M. Fakharzadeh, S. Safavi-Naeini, S. H. Jamali, and P. Mousavi, "Zero-knowledge beamforming of phased array antennas based on simultaneous perturbation gradient approximation," in *Proc. IEEE Int. Symp. Antennas Propag.*, Albuquerque, NM, Jul. 2006, pp. 537–540.
[12] P. Mousavi, M. Fakharzadeh, S. H. Jamali, K. Narimani, M. Hossu, H. Bolandhemmat, G. Rafi, and S. Safavi-Naeini, "A low-cost ultra low profile phased array system for mobile satellite reception using zero-knowledge beamforming algorithm," *IEEE Trans. Antennas Propag.*, vol. 56, no. 12, pp. 3667–3679, Dec. 2008.
[13] T. Kenjo, *Stepping Motors and Their Microprocessor Control*. Oxford, U.K.: Clarendon, 1984.
[14] D. H. Titterton and J. L. Weston, *Strap-Down Inertial Navigation Technology*. London, U.K.: Peregrinus, 1997.
[15] *Analog Devices Products*. [Online]. Available: http://www.analog.com
[16] *Analog Devices ADIS16100 Yaw Rate Gyroscope (with SPI) Datasheet (Initial Version)*. [Online]. Available: http://datasheet.digchip.com/041/041-21720-ADIS16100.pdf
[17] W. Stockwell, *Bias Stability Measurement: Allen Variance*. Beijing, China: Crossbow Technol. Inc.. [Online]. Available: http://www.xbow.com
[18] D. Simon and J. L. Weston, *Nonlinear Estimation*. London, U.K.: Peregrinus, 2005.
[19] M. Zribi and J. Chiasson, "Position control of a PM stepper motor by exact linearization," *IEEE Trans. Autom. Control*, vol. 36, no. 5, pp. 620–625, May 1991.
[20] G. F. Franklin, J. D. Powell, and M. L. Workman, *Digital Control of Dynamic Systems*, 3rd ed. Reading, MA: Addison-Wesley, c1998.
[21] R. O. Schmidt, "Multiple emitter location and signal parameters estimation," *IEEE Trans. Antennas Propag.*, vol. AP-34, no. 3, pp. 276–280, Mar. 1986.

[22] J. Capon, "High resolution frequency-wave number spectrum analysis," *Proc. IEEE*, vol. 57, no. 8, pp. 1408–1418, Aug. 1969.
[23] R. Roy and T. Kailath, "ESPRIT—Estimation of signal parameters via rotational invariance techniques," *IEEE Trans. Acoust., Speech, Signal*, vol. 37, no. 7, pp. 984–995, Jul. 1989.
[24] C. M. Tan, S. E. Foo, M. A. Beach, and A. R. Nix, "Ambiguity in MUSIC and ESPRIT for direction of arrival estimation," *Electron. Lett.*, vol. 38, no. 24, pp. 1598–1600, Nov. 2002.
[25] K. C. Huarng and C. C. Yeh, "Adaptive beamforming with symmetric conjugate weights," *IEEE Trans. Antennas Propag.*, vol. 39, no. 7, pp. 926–932, Jul. 1991.
[26] S. Hayward, "Effects of motion on adaptive arrays," *Proc. Inst. Elect. Eng.—Radar, Sonar Navig.*, vol. 144, no. 1, pp. 15–20, Feb. 1997.
[27] M. Fakharzadeh, H. Jamali, P. Mousavi, and S. Safavi-Naeini, "Fast beamforming for mobile satellite receiver phased arrays: Theory and experiment," *IEEE Trans. Antennas Propag.*, Jun. 2008. accepted for publication.

Hamidreza Bolandhemmat received the M.Sc. degree in aerospace engineering, flight dynamics, and control from the Sharif University of Technology, Tehran, Iran, in 2003. He is currently working toward the Ph.D. degree with the Department of Mechanical and Mechatronics Engineering, University of Waterloo, Waterloo, ON, Canada.

He is a Control Systems Engineer with Intelwaves Technologies Ltd., Waterloo. His research interests include estimation, control, and navigation.

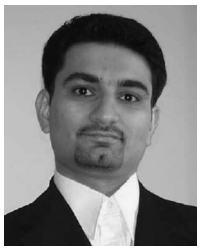

Mohammad Fakharzadeh received the B.Sc. degree (with honors) in electrical engineering from Shiraz University, Shiraz, Iran, and the M.Sc. degree from Sharif University of Technology, Tehran, Iran, in 2000 and 2002, respectively. He is currently working toward the Ph.D. degree with the Intelligent Integrated Radio and Photonics Group, University of Waterloo, Waterloo, ON, Canada.

From January 2003 to September 2004, he was a Faculty Member of the Department Electrical Engineering, Chamran University of Ahvaz, Tehran, where he was evaluated as the best instructor by the undergraduate students of the department. He is also currently with Intelwaves Technologies Ltd., Waterloo. His areas of interest include phased-array design and beamforming, optical delay lines, signal processing, and adaptive filters.

Pedram Mousavi (S'96–M'01) received the B.Sc. (Hons.) degree in telecommunication engineering from Iran University of Science and Technology, Tehran, Iran, in 1995 and the M.Sc. and Ph.D. degrees from University of Manitoba, Winnipeg, MB, Canada, in 1997 and 2001, respectively, all in electrical engineering.

From 2001 to 2003, he was with Sirific Wireless Corporation as a Senior Microwave Engineer, working on the development of multiband Voltage Control Oscillator for various wireless standards. From 2003 to 2004, he was a Postdoctoral Fellow with the Department of Electrical and Computer Engineering and the Centre for Integrated RF Engineering, University of Waterloo, conducting research on low-cost low-profile phased array antenna system for mobile satellite communication. Backed by his research at the University of Waterloo, he founded Intelwaves Technologies, in which he is currently the CEO. Intelwaves Technologies Ltd. is developing a comprehensive suite of smart antenna technologies that can be used to provide satellite television programming and satellite broadband Internet access within moving vehicles, from passenger cars to commercial aircraft. Its vision is to make cars communication centers. His research interests include miniaturized intelligent antennas and radios, microwave and millimeter-wave low-profile/integrated adaptive antenna structures, and emerging technologies for microwave and millimeter waves in smart antennas.

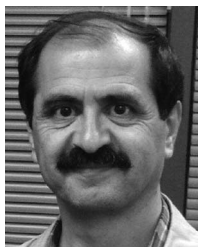

S. Hamidreza Jamali was born in Zanjan, Iran. He received the B.Sc. and M.Sc. degrees from the University of Tehran, Tehran, Iran, in 1978 and 1980, respectively, and the Ph.D. degree from Concordia University, Montreal, QC, Canada, in 1991.

From 1982 to 1983, he was with the Electronics Research and Production Center: a subsidiary of the Iran Broadcast Organization. In 1983, he joined the Department of Electrical and Computer Engineering, University of Tehran, where he is currently an Associate Professor. He has also been a Visiting Professor with the Department of Electrical and Computer, University of Waterloo, Waterloo, ON, Canada, and the Chief Technical Officer of Intelwaves Technologies Ltd., Waterloo, since November 2004. He is the coauthor of a book entitled *Coded Modulation Techniques for Fading Channel* (Kluwer, 1994). His current research interests include multiple-input–multiple-output and smart antenna systems and the applications of coding and diversity techniques to wireless communications.

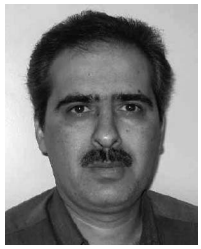

Gholamreza Z. Rafi received the B.Sc. degree in electrical engineering from Isfahan University of Technolgy, Isfahan, Iran, in 1991 and the M.Sc. and Ph.D. degrees in electrical engineering from Amirkabir University of Technology (Tehran Polytechnic), Tehran, Iran, in 1997 and 2000, respectively.

He was an Assistant Professor with the Department of Electrical Engineering, University of Zanjan, Zanjan, Iran, from 2000 to 2001 and collaborated with Iran Telecommunication Center (ITRC) as a Research Scientist. He was a Postdoctoral Fellow with the Department of Electrical and Computer Engineering, University of Manitoba, Winnipeg, MB, Canada, from 2001 to 2004. He was with Intelwaves Technology, Waterloo, ON, Canada, from 2005 to 2008. He is currently with the Department of Electrical and Computer Engineering, University of Waterloo, as a Senior Research Scientist and Antenna Laboratory Manager. His research interests include integration of radio-frequency circuits with antennas and applied electromagnetics.

Safieddin Safavi-Naeini (M'79) was born in Gachsaran, Iran, in 1951. He received the B.Sc. degree in electrical engineering from the University of Tehran, Tehran, Iran, in 1974 and the M.Sc. and Ph.D. degrees in electrical engineering from the University of Illinois, Urbana, in 1975 and 1979, respectively.

He joined the Department of Electrical Engineering, University of Tehran, as an Assistant Professor in 1980 and became an Associate Professor in 1988. He has been a Full Professor with the Department of Electrical and Computer Engineering, University of Waterloo, Waterloo, ON, Canada, since 2002. He has been a scientific and technical consultant to a number of national and international telecommunication industrial and research organizations since 1980. His research interests and activities include numerical electromagnetics applied to radio-frequency/microwave/millimeter-wave systems and circuits, antennas and propagation, wireless communication systems, very-high-speed digital circuits, and optical communication systems.